2022 ACWE 14th Americas Conference on Wind Engineering
May 17-19, 2022 – Lubbock, TX
National Wind Institute – Texas Tech University

A Study of Dynamic Response of a Lighting Pole during a Downburst through time-domain analysis and Full-Scale Structural Monitoring

Mekdes T. Mengistu [a], Maria Pia Repetto [b]

[a] *University of Genova, Genova, Italy, mekdestadesse.mengistu@edu.unige.it*
[b] *University of Genova, Genova, Italy, repetto@dicat.unige.it*

ABSTRACT: The effect of downbursts on structures has been a topic of study for the past two decades. Numerical and analytical methods for the calculation of downburst wind loads and the dynamic response of structures have also been proposed. However, the proposed methods have not been verified using full-scale structural response data. This research presents the response of a monitored lighting pole during two downburst events, with a comparison of responses estimated through time-domain analysis. It is shown that the overall trend of the time history of the mean response is in close agreement with the registered response, and the fluctuating component of the response is highly dependent on the assumed wind field coherence.

KEYWORDS: Downburst, Full-scale monitoring, Time-domain analysis

1 INTRODUCTION

In the past 20 years, many researchers studied the effect of downburst winds on structures. Analytical models for the calculation of loads due to downburst outflow winds were also proposed (Kwon & Kareem, 2009; Solari et. al, 2015; Solari & De Gaetano, 2018). However, due to the small spatial and temporal scale of downbursts, validation of the proposed analytical models through registered structural response has not been sufficiently done. To fill this gap in research, full-scale monitoring of selected three slender structures has been initiated through the European Union-funded project, THUNDERR (Solari et. al, 2020). The aim of the full-scale monitoring is to study the response of simple slender structures under downburst winds and, to conduct a validation study for the previously proposed analytical methods of downburst wind load and dynamic response modeling.

2 DESCRIPTION OF THE MONITORING STATION

The wind and structural response monitoring system is mounted on a 16.6 m lighting pole located at the harbor of La Spezia, Italy (Orlando, 2021). The pole is placed on a 2.5 m concrete cube foundation with a connection resulting in an almost perfect clamped end. The structure is made of two hollow steel shafts by overlapping one on top of the other vertically for an overlap length of 1 m. Both steel shafts are made through the lamination and calendaring process of a 4 mm thick steel sheet, longitudinally welding the edges of the steel sheets to create a 16-sided hollow polygon section. The bottom shaft starts from the base and has a length of 7.75 m. It decreases its maximum cross-sectional dimension from 528 mm at the base to 400 mm at the top. The upper shaft starts

from 6.75 m from the base of the pole and has a length of 9.85 m. It decreases its maximum cross-sectional dimension from 417 mm at the bottom to 254 mm at the top. A steel ladder is attached to the pole on one of the sides of the polygonal shaft and it is interrupted by a rectangular platform at 10 m. At the top of the pole, a square platform houses the anemometer, lighting equipment, and a security camera.

The pole is equipped with a monitoring system for wind and structural response measurement. Figure 1 shows a sketch of the tower (a), the locations of the sensors (b) and the geographical and inertial reference systems (c). A triaxial ultrasonic anemometer measuring wind speed at a frequency of 10 Hz is installed at 21.7 meters above the ground. Two biaxial accelerometers measuring acceleration at a frequency of 200 Hz are installed on one of the sides of the polygonal shafts at 10.5 m (Ax_2, Ay_2) and 16.6 m (Ax_1, Ay_1) from the base of the pole. Eight monoaxial strain gauges measuring strain at a frequency of 100 Hz are installed at 0.5 m (S_A, S_B, S_C, S_D) and 1.5 m (S_E, S_F, S_G, S_H) above the base of the pole on 4 sides of the polygonal shaft. The strain gauges and accelerometers are placed on the sides of the polygonal shaft in such a way that response is measured in two orthogonal directions.

3 CASE STUDIES OF DOWNBURSTS SELECTED FOR ANALYSIS

In this paper, two downburst events whose wind and structural response data have been registered by the monitoring system are selected. Figures 2a and 2c show 1 hour time history of instantaneous and running mean wind speed averaged over 10 minutes whereas Figures 2b and 2d show instantaneous and running mean wind direction averaged over 10 minutes during the two events. The North is set as 0^0 azimuths in the wind direction measurement, while the East is 90^0 with subsequent values in the clockwise direction.

The first event occurred on April 04, 2019, and had a maximum instantaneous wind speed of 22.5 m/s. The wind direction changed from approximately 0 to 90 degrees in a time span of about 20 minutes. The presence of significant wind before the occurrence of the ramp-up of the downburst is due to a background atmospheric boundary layer (ABL) wind that has been blowing from a couple of days before.

The second event occurred on October 02, 2019, and had a maximum instantaneous wind speed of 20.5 m/s. From Figure 2c it can be observed that the wind speed increased significantly from approximately 2 m/s to 20.5 m/s in 10 minutes. In addition, there is a significant change in wind direction of about 180 degrees during the ramp-up in wind speed.

The structural response was registered by the strain gauges and accelerometers. Figures 3 and 4 show 10 minutes time history of instantaneous and mean wind speed (a), instantaneous wind direction (b), resultant of strain measured by strain gauge S_A and S_B (c), and acceleration measured by accelerometers A_{x2} and A_{y2} (d). It is evident that the trend of the mean strain is closely similar to the trend of mean wind speed, and the amplitude of acceleration is correlated with the intensity of the wind speed, increasing from nearly zero to a higher amplitude with the increase in wind speed.

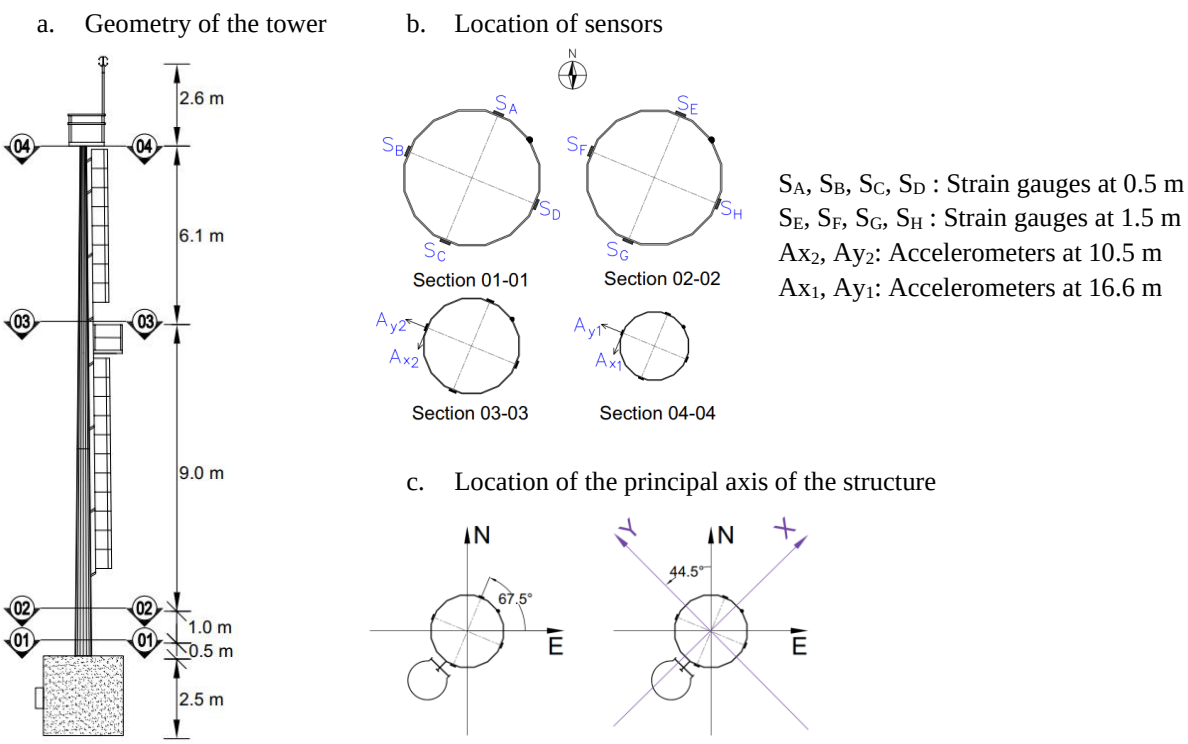

Figure 1. The geometry of the lighting pole and monitoring sensors locations

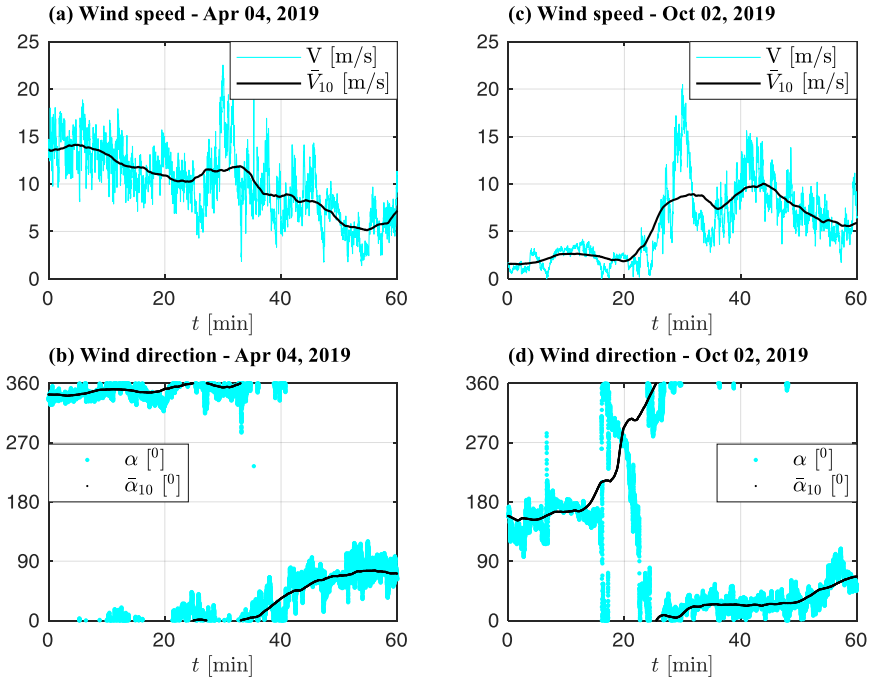

Figure 2. 1 hr time history of wind speed and direction for the two downbursts

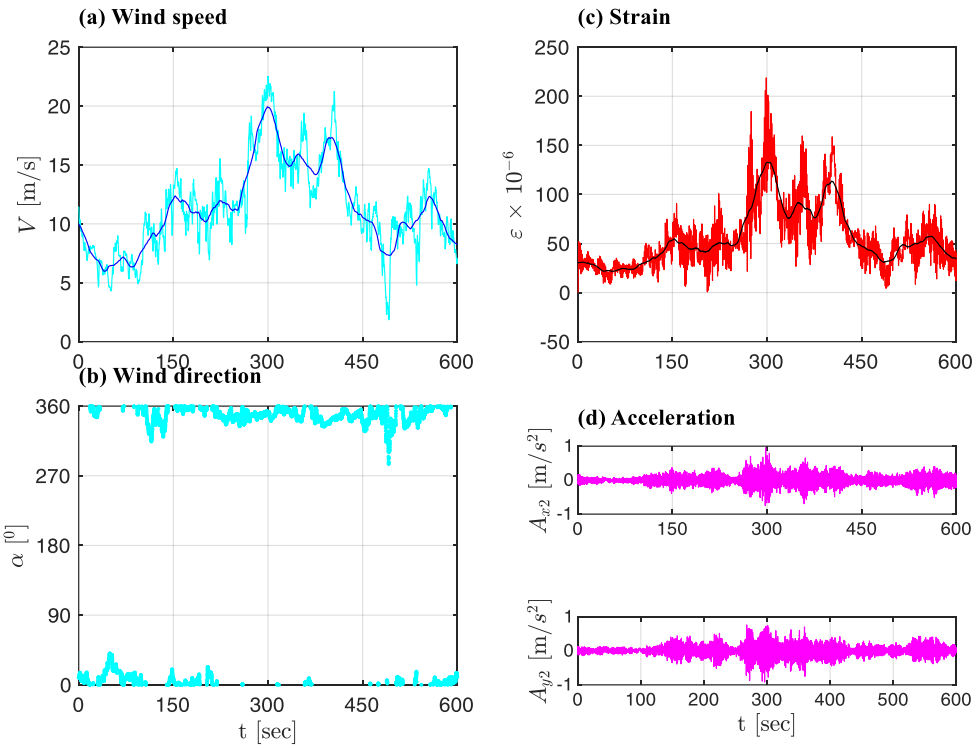

Figure 3. Wind and structural response for the downburst on April 04, 2019

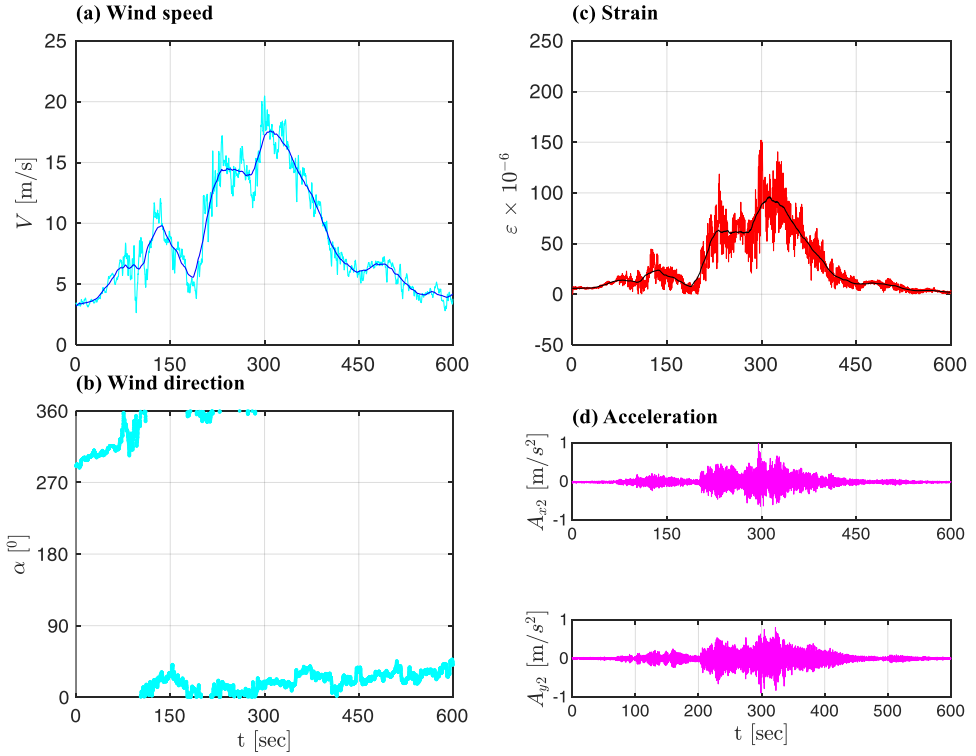

Figure 4. Wind and structural response for the downburst on October 02, 2019

4 RESPONSE CALCULATION USING TIME-DOMAIN ANALYSIS

4.1 *Wind speed decomposition*

Decomposition of horizontal wind speed into a mean and fluctuating component is a common procedure in synoptic winds to study the mean static and dynamic response of structures separately. The same procedure is not trivial for downburst winds due to the transient nature of the event and the non-Gaussian distribution of the wind velocity.

Zhang et. al (2019) proposed a new approach for thunderstorm winds in which the wind speed is decomposed into slowly-varying mean and fluctuating components in the alongwind direction and fluctuating components in the crosswind direction. This enabled the estimation of alongwind and crosswind response and consideration of the change in angle of attack in time domain analysis (Brusco et.al, 2019). Therefore, this approach is considered to be suitable to decompose wind speed for the two registered downburst events.

Initially slowly varying mean wind speeds averaged over 30 seconds are extracted from the instantaneous wind speed registered in the East , $V_E(t)$, and North directions, $V_N(t)$.

$$V_E(t) = \bar{V}_E(t) + V'_E(t) \tag{1}$$

$$V_N(t) = \bar{V}_N(t) + V'_N(t) \tag{2}$$

where $\bar{V}_E(t)$ and $\bar{V}_N(t)$ are slowly varying mean wind speed components extracted here by a running mean filter with a moving average period T = 30s whereas $V'_E(t)$ and $V'_N(t)$ are the residual turbulent fluctuations.

These mean wind speed components are vector-summed to obtain the resultant slowly varying mean wind speed, $\bar{u}(t)$ and its direction, $\bar{\beta}(t)$.

$$\bar{u}(t) = \sqrt{\bar{V}_E^2(t) + \bar{V}_N^2(t)} \tag{3}$$

$$\bar{\beta}(t) = a\tan 2\left[\frac{\bar{V}_N(t)}{\bar{V}_E(t)}\right] \tag{4}$$

Accordingly, $V'_E(t)$ and $V'_N(t)$ are projected on new orthogonal axes (*x*,*y*) in which the *x*-axis is aligned with the mean wind speed.

$$u'(t) = V'_E(t)\cos\bar{\beta}(t) + V'_N(t)\sin\bar{\beta}(t) \tag{5}$$

$$v'(t) = -V'_E(t)\sin\bar{\beta}(t) + V'_N(t)\cos\bar{\beta}(t) \tag{6}$$

The alongwind and crosswind fluctuating components, $u'(t)$ and $v'(t)$ respectively, are further decomposed as a multiplication between their standard deviation, $\sigma_u(t)$ and $\sigma_v(t)$, and rapidly varying stationary Gaussian components, $\tilde{u}'(t)$ and $\tilde{v}'(t)$.

$$u'(t) = \sigma_u(t)\tilde{u}'(t) \tag{7}$$

$$v'(t) = \sigma_v(t)\tilde{v}'(t) \tag{8}$$

Thus, the alongwind (*x*-direction) and crosswind (*y*-direction) components of the wind speed are expressed as:

$$u(t) = \bar{u}(t) + u'(t) = \bar{u}(t)\left[1 + I_u(t)\tilde{u}'(t)\right] \tag{9}$$

$$v(t) = v'(t) = \bar{u}(t)\left[I_v(t)\tilde{v}'(t)\right] \tag{10}$$

where the longitudinal and lateral slowly varying turbulence intensities, $I_u(t)$ and $I_v(t)$, are given by:

$$I_\varepsilon(t) = \sigma_\varepsilon / \bar{u}(t) \tag{11}$$

with $\varepsilon = u,v$.

4.2 *Wind field*

The structural monitoring system has only one anemometer at 21.7 m above the ground and as a result distribution of wind speed in the vertical direction was not registered. Thus the wind speed time history should be calculated at different heights of the structure from the reference time history of wind speed registered at the anemometric location, assuming suitable models for mean wind profile, turbulence intensity profile and turbulence coherence. From Equation 9 and Equation 10, wind speed in the alongwind and crosswind direction has three components, i.e., mean wind speed, turbulence intensity, and reduced fluctuating component. For the mean wind speed, the model proposed by Wood et.al (2001) was applied to the mean wind speed time history registered by the anemometer to calculate the time-varying mean wind speed at different locations in the vertical direction. On the other hand, an equivalent reduced fluctuating component of wind speed identically coherent in space was obtained applying the equivalent wind spectrum technique (Solari, 1988) on the reference reduced fluctuating component. Although turbulence intensity is time-varying and non-uniform in the vertical direction (Canepa et. al, 2020), a refined model for turbulence intensity is not proposed in the literature. Thus, the turbulence intensity was assumed to be slowly varying in time but constant in the vertical direction. The implication of this assumption is that turbulence intensity in the vertical direction is the same as the reference turbulence intensity registered by the anemometer. Having all these three wind speed components, the total wind speed in the alongwind and crosswind direction was obtained at various heights of the structure.

4.3 *Aerodynamic force*

As explained in the previous section, equivalent wind speed over the height of the structure is generated in the alongwind and crosswind directions. These two wind components were vector-summed and their resultant, *U(z, t),* is used to calculate the drag and lift forces with the assumption of the strip and quasi-steady theory.

$$f_d(z,t) = 0.5\rho b(z)U^2(z,t)c_d \tag{12}$$

$$f_l(z,t) = 0.5\rho b(z)U^2(z,t)c_l \tag{13}$$

where, $f_d\ (z,t)$ is the drag force, $f_l(z,t)$ is the lift force, c_d is the drag coefficient, c_l is the lift coefficient, ρ is the air density, and $b(z)$ is the cross-sectional width of the structure.

Selecting the appropriate values of aerodynamic coefficients for the calculation of the aerodynamic force was found to be a delicate issue. The inherent nature of thunderstorm winds with a sudden increase in wind speed mostly coupled with a change in angle of attack, calls for a detailed investigation on this aspect of uncertainty. Although the applicability of constant aerodynamic coefficients in the 10-minute time span needs further assessment, in this study, a constant value of drag and lift coefficients were applied for every instant of time. These constant aerodynamic coefficients were selected from the range of values obtained through wind tunnel

testing based on the condition that the final mean response calculated using time-domain analysis has a minimum root mean square error when it is compared with the mean registered response.

To solve the equation of motion in the principal bending directions of the structure, the drag and lift forces were finally projected on the principal axes of the structure to obtain $f_X(z,t)$ and $f_Y(z,t)$.

4.4 *Dynamic response*

The natural frequency and modal shape of the structure were obtained through operational modal analysis. For this research, only the first two bending modes are considered. The first and the second modes are bending modes with single curvature in the *Y* and *X* directions respectively, where *Y* and *X* are principal orthogonal axes as shown in Figure 1c. The modal shape is approximated by a power function $(z/H)^k$ where *z* is the height above the base and *H* is the total height of the pole, i.e, 16.6 m and *k* is a proper value obtained from operational modal analysis Table 1 lists the dynamic properties of the structure in the two principal directions.

Table 1. Dynamic properties of the monitored structure

Mode	Natural frequency (Hz)	Mode shape		Modal mass (kg)
1st	0.75	$(z/H)^{1.9}$	Bending in the *Y* direction	649
2nd	0.85	$(z/H)^{1.6}$	Bending in the *X* direction	673

From modal analysis, the *X* and *Y* uncoupled and orthogonal component of the response, q_X and q_Y, are given by

$$q_i(z,t) = \psi_{1,i}(z)\, p_{1,i}(t) \tag{14}$$

where $i=X,Y$, $\psi_{1,X}$ and $\psi_{1,Y}$ are the 1st bending mode shapes; $p_{1,X}$ and $p_{1,Y}$ are the 1st principal coordinates in the *X* and *Y* directions.

The *i-th* principal coordinate is obtained by solving the equation of motion in the principal direction:

$$\ddot{p}_{1,i}(t) + 2\xi_{1,i}\omega_{1,X}\,\dot{p}_{1,i}(t) + \omega_{1,i}^2\, p_{1,i}(t) = \frac{1}{m_{1,i}}\, f_{1,i}(t) \tag{15}$$

where $m_{1,i}$ and $f_{1,i}$ are 1st mode mass and 1st mode aerodynamic wind force, respectively, in the *i-th* direction, given by.

$$m_{1,i} = \int_0^H m(z)\psi_{1,i}^2(z)\,dz \tag{16}$$

$$f_{1,i}(t) = \int_0^H f_i(t,z)\psi_{1,i}(z)\,dz \tag{17}$$

where $m(z)$ is the mass per unit length; $f_i(t, z)$ is the aerodynamic wind force per unit length in the *i-th* direction.

The equation of motion was solved in the time domain using the state space method at a time step of 0.1 seconds without considering aeroelasticity.

5 CALCULATION OF DEFLECTION FROM STRAIN GAUGE READINGS

The calculation of top displacement from strain gauge readings was done by assuming elastic bending and applying the Bernoulli-Euler beam equation for small deflection with flexure theory for the first two single curvature bending modes. In particular, the strain gauge readings were projected on the principal axes of the structure (*X* and *Y*) and the principal coordinates of the displacement in the two principal directions were calculated using the equation:

$$p_{1,i}(t) = \frac{\varepsilon_i(t,z)}{r(z)\dfrac{d^2\psi_{1,i}}{dz^2}} \tag{18}$$

where $\varepsilon_i\ (t, z)$ is strain readings projected on the *i-th* principal direction; *r* is the distance to the centroid of the geometry.

Since the monitored structure is not prismatic, the distance to the centroid varies with height; $r(z)$ is 257.9 mm at 0.5 m from the base of the structure where strain gauges S_A-S_D are installed and $r(z)$ is 249.65 mm at 1.5 m from the base of the structure where the strain gauges S_E-S_H are installed. On the other hand, the modal shape is approximated by a power function $\psi_{1,i}=(z/H)^{ki}$ whose second derivative is

$$\frac{d^2\psi_{1,i}}{dz^2} = k_i(k_i-1)\left(\frac{z}{H}\right)^{k_i-2}\frac{1}{H^2} \tag{19}$$

Once principal coordinates of displacement in the two principal directions, $p_{1,X}(t)$ and $p_{1,Y}(t)$, are calculated, the deflection at any height of the structure can be obtained using Equation (14).

6 RESULTS AND DISCUSSION

The time-domain analysis was done considering the uncertainty of structural damping ratio and coherence of wind speed fluctuation in the vertical direction. Damping ratios of 0.2% , 0.5% and 1% were considered. Partially coherent fluctuating wind component obtained through Equivalent wind spectrum method considering exponential decay coefficients recommended for synoptic winds (Solari & Piccardo, 2001) as well as perfect correlation were considered.

From the comparison between top displacement obtained through time-domain analysis and registered response obtained from strain gauges, it was observed that the calculated and registered responses share a similar trend for the considered aerodynamic coefficients. The complete analysis will be presented in future publications.

Considering in particular the fluctuating component of the response, its dependency on the damping value and level of coherence is discussed by comparing the standard deviation of the fluctuating part of the response for the calculated and registered time history. Figures 5 and 6 show a comparison of standard deviation in the alongwind (*x*) and crosswind (*y*) direction assuming partial (a and b) and perfect correlation (c and d) of wind field in the vertical direction, for different values of damping. It is evident that the assumption of partial correlation with exponential decay coefficients recommended for synoptic events underestimates the standard deviation of fluctuating response. Especially for the downburst event of October 02, it can be seen that the standard deviation of the registered response fluctuation is higher than its calculated counterpart regardless of the different assumptions of damping and coherence.

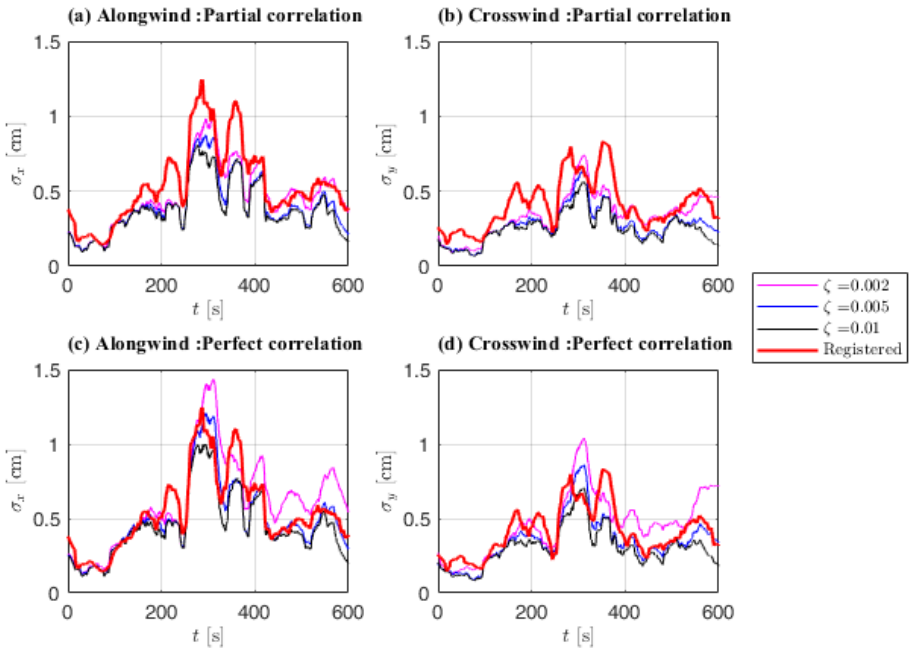

Figure 5. Standard deviation of fluctuating response for the downburst on April 04, 2019

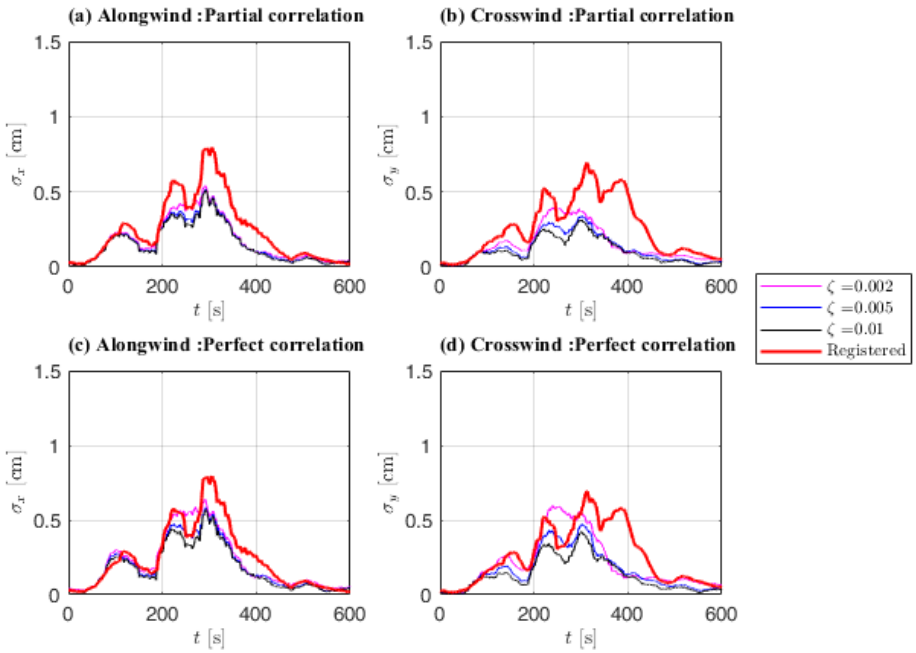

Figure 6. Standard deviation of fluctuating response for the downburst on October 02, 2019

7 CONCLUSION

The dynamic response of a lighting pole during two downburst events has been studied using time domain analysis and registered structural response. Comparison was made on the dynamic response time history. For the considered aerodynamic coefficients, the general trend of the registered and calculated response was found to have comparable trend with a difference in

magnitude depending on the assumed damping and turbulence coherence parameters. Although the damping ratio has always been known to be a governing parameter in the dynamic response of structures, the assumption of a level of correlation between wind speed fluctuations at different heights of the structure was found to be an additional uncertain parameter that dictates the total response of the structure. The application of exponential decay coefficients recommended for synoptic winds in modeling the coherence of wind field in the vertical direction underestimated the total response and the standard deviation of the response fluctuation. Thus, further studies on the coherence of the wind field during a downburst are highly essential to properly estimate the response of structures during a downburst.

8 ACKNOWLEDGMENTS

This research is funded by European Research Council under the European Union's Horizon 2020 research and innovation program (Grant Agreement No. 741273) for the project THUNDERR - Detection, simulation, modelling and loading of thunderstorm outflows to design wind safer and cost-efficient structures—through an Advanced Grant 2016. The monitoring system is co-funded by the Italian Ministry of Instruction and Scientific Research (MIUR), Prot. 2015TTJN95 in the framework of the Research Project of Relevant National Interest (PRIN 2015).

9 REFERENCES

S. Brusco, V. Lerzo, & G. Solari (2019). Directional response of structures to thunderstorm outflows. Meccanica, 54(9), 1281-1306.

F. Canepa, M. Burlando, G. Solari (2020). Vertical profile characteristics of thunderstorm outflows. Journal of Wind Engineering and Industrial Aerodynamics, 206

D.K. Kwon & A. Kareem (2009). Gust-front factor: New framework for wind load effects on structures. Journal of Structural Engineering,135(6),717-732

A. Orlando (2021). Full scale monitoring of the wind induced response of vertical slender structures, with fixed and roatating masses. Ph.D. Thesis, Universita degli Studi di Genova

G. Solari (1988). Equivalent wind spectrum technique: Theory and applications. Journal of Structural Engineering, 114(6), 1303-1323

G. Solari, M. Burlando, M.P. Repetto (2020). Detection, simulation, modeling, and loading of thunderstorm outflows to design wind-safer and cost-efficient structures. Journal of Wind Engineering and Industrial Aerodynamics, 200, 104142

G. Solari & G. Piccardo (2001). Probabilistic 3-D turbulence modeling for gust buffeting of structures. Probabilistic Engineering Mechanics, 16(1), 73-86

G. Solari, P. De Gaetano & M.P. Repetto (2015). Thunderstorm response spectrum: Fundamentals and case study. Journal of wind Engineering and Industrial Aerodynamics, 143,62-77

G. Solari, D. Rainisio & P. De Gaetano (2017). Hybrid simulation of thunderstorm outflows and wind-excited response of structures. Meccanica, 52(13), 3197-3220

G. Solari, & P. De Gaetano (2018). Dynamic response of structures to thunderstorm outflows: Response spectrum technique vs time-domain analysis. Engineering Structures, 176,188-207

G.S. Wood, K.C.S. Kwok, N.A. Motteram & D.F. Fletcher (2001). Physical and numerical modeling of thunderstorm downbursts. Journal of Wind Engineering and Industrial Aerodynamics, 89(6), 535-552.

S. Zhang, G. Solari, M. Burlando & Q. Yang (2019). Directional decomposition and properties of thunderstorm outflows. Journal of Wind Engineering and Industrial Aerodynamics, 189, 71-90